Composites Part C: Open Access 5 (2021) 100147

Contents lists available at ScienceDirect

Composites Part C: Open Access

journal homepage: www.elsevier.com/locate/jcomc

Transverse damage in glass fiber reinforced polymer under thermo-mechanical loading

David Kraus[1], Volker Trappe*

Federal Institute for Materials Research and Testing (BAM), Unter den Eichen 87, 12205 Berlin, Germany

ARTICLE INFO

Keywords:
Glass fiber reinforced polymer
Thermo-mechanics
Fatigue
Damage, composite
Temperature

ABSTRACT

In this study, the thermomechanical damage behavior of a glass fiber reinforced polymer material is investigated. The coefficients of thermal expansion of the composite as well as the matrix are measured in a wide temperature range. Quasi-static experiments with neat resin, unidirectional and multidirectional laminates are performed as well as fatigue experiments in a temperature range from 213 K to 343 K. This study focusses on the matrix damage due to fiber-parallel loading. A correlation between matrix effort, the dilatational strain energy of the matrix and the damage state of the specimen is demonstrated. It is shown that a fatigue life assessment can be performed with the aid of a temperature-independent master fatigue curve.

1. Introduction

Fiber reinforced polymer (FRP) structures are widely established in lightweight applications, such as wind energy or aerospace. These structures are often loaded in a wide temperature range. The operating temperature of a thermoset polymer matrix composite affects three major points:

- The elastic properties, mainly of the matrix, change with temperature. Lower temperatures lead to a higher stiffness and strength of the matrix, while higher temperatures decrease the elastic properties. In the glass transition zone, a drastic change from glassy to rubbery behavior is observed.
- Macro-mechanical residual stresses are introduced into multi-angle laminates caused by the orthotropic thermal expansion behavior of each layer.
- Micro-mechanical residual stresses inside each unidirectional layer are caused by the different coefficients of thermal expansion (CTE) of the fiber and matrix material [1].

The temperature-dependence of the mechanical properties of thermoset polymer materials is well known. Fiedler et al. investigated the strength and stiffness of different common epoxy matrix systems, subjected to various temperatures. They proposed a linear relationship between the elastic modulus of the epoxy and the operating temperature in the thermal range considerably below the glass transition temperature [2].

The properties of glass fibers, on the other hand, are shown to be independent of changes in temperature up to 300 °C [3]. For carbon fibers, no significant loss in strength and stiffness has been observed up to 1000 °C [4].

The macro-mechanical thermal residual stresses between differently orientated layers can be treated as thermal loads in terms of Classical Lamination Theory (CLT) [5].

The general prediction of damage initiation inside the matrix under quasi-static short time loading is possible using well-known failure criteria. Established criteria like the Puck criterion [6] predict fiber as well as inter-fiber failure inside a composite material. However, Puck's criterion is based on the stresses of each composite layer and does not consider the micro-mechanical stress state of the matrix. Hence, the impact of residual stresses is not considered. Krimmer [7,8] proposed a micro-mechanical analytical framework which allows for the calculation of a three dimensional in-situ stress state of the matrix on the level of filament-matrix interaction. Relating the matrix in situ stress to its strength, Krimmer proposed a failure criterion for matrix damage onset.

In the frame of an extensive study [9], the damage evolution and fatigue behavior of a glass fiber reinforced polymer was experimentally investigated. This paper focusses on the damage in transverse layers. For more detailed conclusions on the temperature-dependent damage behavior of fiber reinforced polymer materials, experiments with multiaxial mechanical loading are required. For this purpose, tubular specimens are favored since the undesired free-edge effect can be avoided. Investigations on tubular specimens under combined tension-torsion load as performed e.g. by Adden and Horst [10] or under internal pressure load as described by Munzke et al. [11] may lead to promising results at

* Corresponding author.
E-mail address: volker.trappe@bam.de (V. Trappe).
[1] With BAM until 03/2019

https://doi.org/10.1016/j.jcomc.2021.100147
Received 7 February 2021; Received in revised form 15 April 2021; Accepted 17 April 2021

warm or cold temperature conditions and shall be performed in future studies.

The data, experimentally obtained in this study for transverse loading, is compared to calculations performed with Krimmer's model, which is extended to consider the impact of temperature on the elastic properties and the residual stresses of the FRP.

In the experimental part of this study, the following experiments have been performed:

- The elastic properties of the matrix and the unidirectional layers of the FRP were determined in a range of 213 K to 343 K by means of tensile tests.
- The CTEs of the matrix and the composite were determined by dilatometry.
- The damage initiation and evolution of 0°/90°-laminates under tensile loads was investigated by means of optical greyscale analysis.
- S-N-curves were generated at different temperatures in the range from 273 K to 343 K and the damage behavior under cyclic loading was investigated.

The data shows a good correlation with the modelling and indicates a relationship between the matrix effort and the damage and failure behavior.

2. Materials and methods

A challenge in the field of composite materials research is the lack of available material data that is complete, in particular for temperature-dependent properties. Therefore, the properties of the composite have been investigated extensively by experiment. All experiments have been conducted with glass fiber reinforced polymer (GFRP) specimens or neat resin specimens. The GFRP specimens consist of Advantex SE 1500 glass fibers with the Hexion RIMR135/RIMH137 epoxy resin system. This material combination is commonly used in the wind energy industry for the production of rotor blade shells.

2.1. Specimen preparation

A combined filament winding and vacuum infusion process has been developed to produce the specimens. The process allows the manufacturing of specimens with variable fiber-matrix combinations.

In the first step, the preform is produced by winding the dry fiber around a frame as shown in Fig. 1. Laminates with multidirectional fiber orientations can be produced by rotating the frame between the winding of two layers. The fibers at the front side of the frame are then fixed with the help of a magnetic frame, which is shown in Fig. 2. These fibers are subsequently impregnated with the resin using a vacuum infusion tool, that is shown in Fig. 3. A transparent cover glass allows the monitoring of the infusion process. The thickness of the cavity and therefore the fiber volume fraction of the produced plate is continuously adjustable by moving the height of the bottom plate of the tool. The closed mold guarantees a smooth surface and good planarity of the specimens.

No textile preform is needed during this manufacturing process and therefore the fiber undulation is very low compared with woven and non-crimp fabrics.

All specimens have been cured at room temperature for at least 48 h in the mold. After demolding, the specimens have been cured for 15 h at 80 °C. The fiber volume fraction ϕ of all specimens is approximately at $\varphi \approx 0.55$.

2.2. Experiments

To assess the thermo-mechanical damage behavior of the material, the following tests were performed:

- The CTEs α_T of the neat resin as well as of the longitudinal and transversal unidirectionally reinforced composite have been determined by dilatometry.

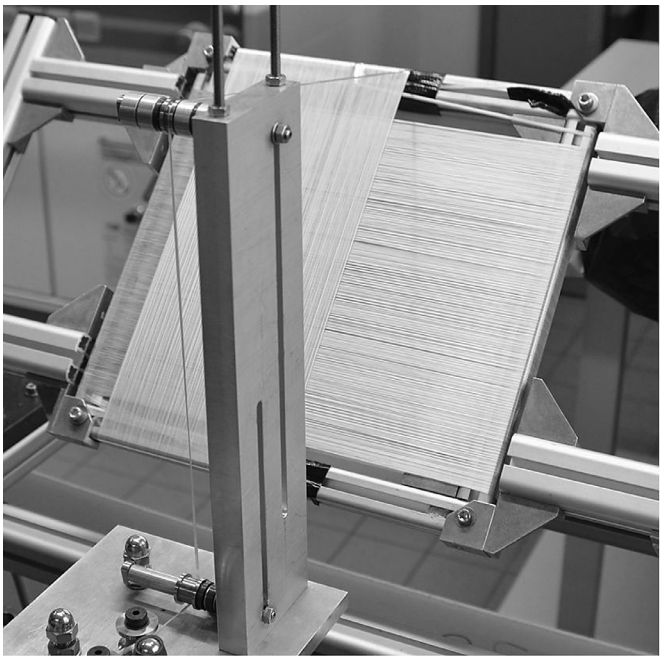

Fig. 1. Filament winding of the dry fibers.

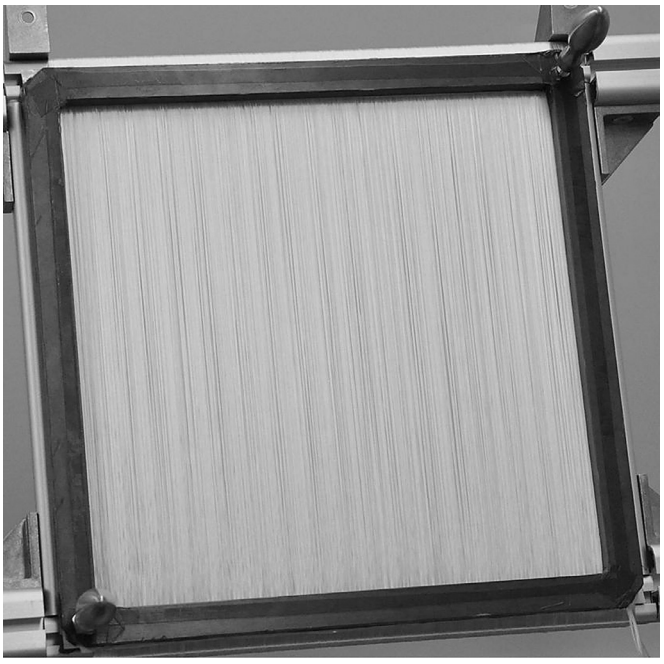

Fig. 2. Clamping of the unimpregnated layers with a magnetic frame.

- Tensile tests on neat resin specimens have been conducted according to ISO 527-2:2012-02 [12] in the temperature range from 213 K to 343 K. The strain has been measured on some specimens using strain gauges, on others with an extensometer to assess the undesired reinforcing effect of the strain gauges [13,14] on the low-modulus epoxy resin. Additional tests at room temperature have been performed with the optical strain measurement system GOM Aramis.
- Static tensile tests were performed on 90° unidirectional reinforced specimens to assess the transverse strength and modulus of the material. The strain was measured using strain gauges. The tests have been performed according to ISO 527-5:2009-07 [15] in five temperature steps from 213 K to 343 K.

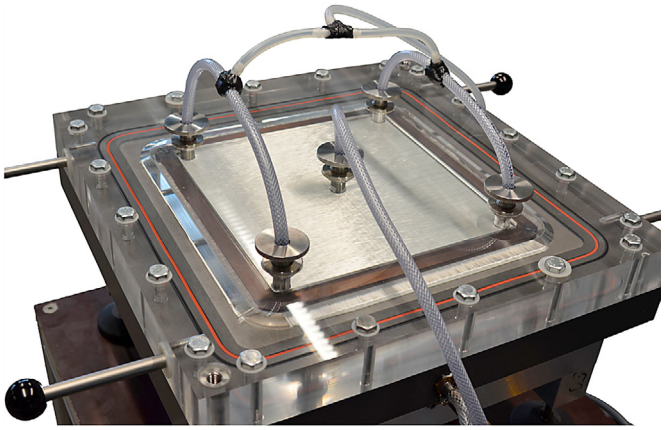

Fig. 3. Vacuum infusion tool.

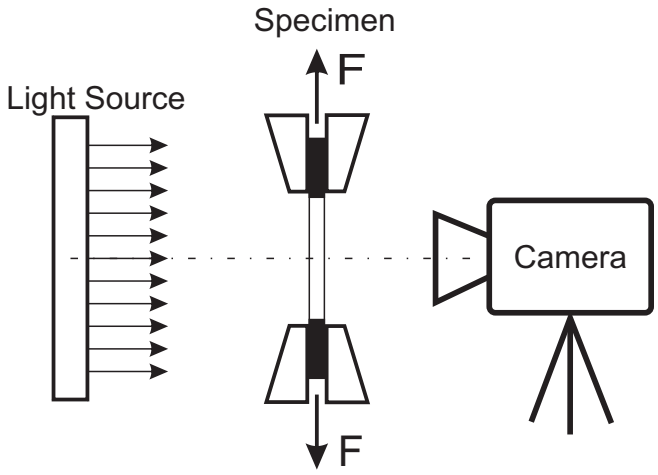

Fig. 4. Light absorption measurement setup.

- Tensile tests have been also carried out with 0°/90° biaxial reinforced specimens in the temperature range of 253 K to 343 K. To monitor the damage evolution, a light absorption analysis [16] was performed. The setup is sketched in Fig. 4. The translucent GFRP specimen was placed between a light source and a camera, and pictures were taken frequently.

Based on its intensity, i.e., darkness, each pixel of the region of interest is given a value between 0 and 255. Here, 0 corresponds to a totally black pixel and 255 to a white pixel. By calculating the mean value of all pixels, the Intensity I is calculated for the specimen and I_{ref} for a reference section in the pictures background to eliminate small variations in the lighting of the picture. A progressive damage in the specimens will then correspond with a change of the damage parameter D for the Load step N:

$$D(N) = 1 - \frac{I(N)}{I(0)} \cdot \frac{I_{ref}(0)}{I_{ref}(N)} \tag{1}$$

Other methods of obtaining the damage parameter also exist. It can be obtained for instance directly from the stress-strain curves of a static test by a method presented by Abu Farsakh et al. [17] or by X-ray refraction, as presented by Trappe et al. [18].

- In addition to the quasi-static tests, tension-tension fatigue tests have been carried out with 0°/90° reinforced specimens in the temperature range from 253 K to 343 K. All fatigue tests have been performed with a load ratio of $R = 0.1$.
- The mechanical properties of the pure glass fiber are taken from the technical datasheet provided by the manufacturer.

3. Theory

Since a correlation between quasi-static and fatigue damage in FRPs and the stress-state in the matrix has already been shown [16,19,20], this study focusses on the matrix stress inside the composite material and the influence of thermal loads on the stiffness, stresses and damage behavior of the composite.

The calculation of matrix stresses inside an FRP is possible using several numerical and analytical models from literature. Here, the in-situ stress state of the matrix of a loaded FRP material has been calculated using the analytical micro-mechanical model published by Krimmer [7,8]. However, the calculation of the matrix stress state with different approaches should lead to similar results. The linear-elastic model allows a relatively simple implementation for practical applications. However, viscoelastic effects at higher temperatures are not considered. Krimmer considers the strain-blocking effect of the fibers, which leads to an orthotropic in-situ behavior of the matrix on a micro-mechanical scale. A hexagonal packing of the fibers is suspected, which led to good results for Müller et al. [16], though in reality the fibers are distributed more stochastically. According to Krimmer, the in-situ matrix stress due to mechanical loading of a composite layer $\sigma_{M,mech}$ results to [8]:

$$\left\{\sigma_{M,mech}\right\} = \begin{Bmatrix} \sigma_{M,1} \\ \sigma_{M,2} \\ \sigma_{M,3} \\ \tau_{M,23} \\ \tau_{M,31} \\ \tau_{M,21} \end{Bmatrix} = \begin{Bmatrix} \dfrac{\frac{\sigma_{E,1}}{E'_{\parallel}} E'_{M\parallel}}{\frac{\sigma_{E,2}}{E'_{\perp}\left(\frac{\sqrt{2\sqrt{3}\frac{\varphi}{\pi}}}{E_F} + \frac{1-\sqrt{2\sqrt{3}\frac{\varphi}{\pi}}}{E'_{M\perp}}\right)}} \\ \dfrac{\sigma_{E,3}}{E'_{\perp}\left(\frac{\sqrt{2\sqrt{3}\frac{\varphi}{\pi}}}{E_F} + \frac{\sqrt{3}-\sqrt{2\sqrt{3}\frac{\varphi}{\pi}}}{E'_{M\perp}}\right)} \\ \dfrac{\tau_{E,23}}{G'_{\perp\perp}\left(\frac{\sqrt{2\sqrt{3}\frac{\varphi}{\pi}}}{G_F} + \frac{1-\sqrt{2\sqrt{3}\frac{\varphi}{\pi}}}{G'_{M\perp\perp}}\right)} \\ \dfrac{\tau_{E,31}}{G'_{\parallel\perp}\left(\frac{\sqrt{2\sqrt{3}\frac{\varphi}{\pi}}}{G_F} + \frac{\sqrt{3}-\sqrt{2\sqrt{3}\frac{\varphi}{\pi}}}{G'_{M\parallel\perp}}\right)} \\ \dfrac{\tau_{E,21}}{G'_{\parallel\perp}\left(\frac{\sqrt{2\sqrt{3}\frac{\varphi}{\pi}}}{G_F} + \frac{1-\sqrt{2\sqrt{3}\frac{\varphi}{\pi}}}{G'_{M\parallel\perp}}\right)} \end{Bmatrix} \tag{2}$$

Here, the external mechanical loads introduced into the layer, σ_E and τ_E, can be obtained from the CLT. The mechanical properties of the fiber E_F and G_F are taken from the technical data sheet. The calculation of the in-situ elastic moduli of the matrix E'_M and the shear moduli G'_M in fiber parallel direction $\parallel$ and transverse direction $\perp$ as well as the moduli of the unidirectional layer E' and G' is explained by Krimmer [7,8].

For the micro-mechanical residual stresses inside the unidirectional layer, which are caused by the different CTEs of the matrix and the fiber, an additional term is added to Eq. 2. Hence, the total matrix stress results to:

$$\left\{\sigma_M\right\} = \left\{\sigma_{M,Mech}\right\} + \begin{Bmatrix} E'_{M\parallel} \int_{T_0}^{T} \left(\alpha_{T,\parallel} - \alpha_{T,M}\right) dT \\ (1-\varphi) E'_{M\perp} \int_{T_0}^{T} \left(\alpha_{T,\perp} - \varphi \frac{E_F}{E_F + E_M} \alpha_{T,F} - \alpha_{T,M}\right) dT \\ (1-\varphi) E'_{M\perp} \int_{T_0}^{T} \left(\alpha_{T,\perp} - \varphi \frac{E_F}{E_F + E_M} \alpha_{T,F} - \alpha_{T,M}\right) dT \\ 0 \\ 0 \\ 0 \end{Bmatrix} \tag{3}$$

Here, $\alpha_{T,\parallel}$ and $\alpha_{T,\perp}$ are the CTEs of the unidirectional layer in the longitudinal and transverse direction, and $\alpha_{T,F}$ and $\alpha_{T,M}$ indicate the CTEs of the fiber and of the matrix.

The residual stresses derived by Eq. 3 have been compared to Finite-Element-Method (FEM) calculations and a good agreement between the analytical calculations and the FEM results was found [9].

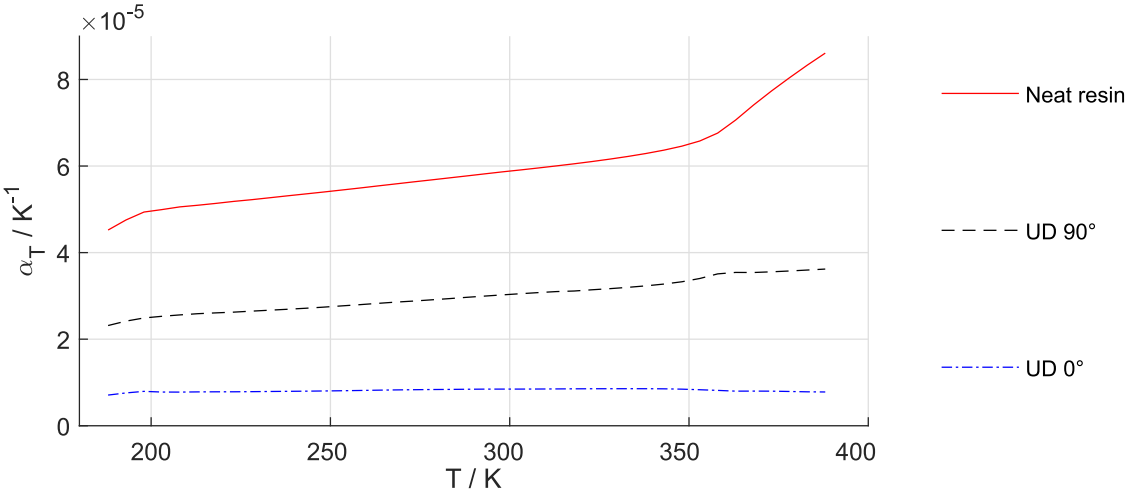

Fig. 5. Dilatometer measurements of the CTEs of neat resin and unidirectional (UD) reinforced composite specimens.

A fracture criterion for the matrix can be derived from the in-situ stress. Krimmer proposes a fracture criterion according to Beltrami [7,8,21], to calculate a matrix effort e_M:

$$e_M = \frac{\sigma_{v,Beltr}}{R_M} \tag{4}$$

For values of $e_M > 1$, matrix cracking is expected. Here, R_M is the strength of the matrix obtained by tensile tests and $\sigma_{v,Beltr}$ is the effective stress according to Beltrami:

$$\sigma_{v,Beltr} = \sqrt{\sigma_I^2 + \sigma_{II}^2 + \sigma_{III}^2 - 2\nu(\sigma_I\sigma_{II} + \sigma_{II}\sigma_{III} + \sigma_{III}\sigma_I)} \tag{5}$$

with the principal stresses $\sigma_I \ldots \sigma_{III}$ of the matrix stress vector $\{\sigma_M\}$ and the Poisson's ratio of the matrix ν.

In this study, the authors propose a criterion different to the Beltrami criterion to assess the transverse damage behavior of the composite. Asp et al. discovered cracking under fiber-parallel load caused by micro-cavitation of the matrix, when the dilatational strain energy of the matrix U_v reaches a critical value [22–24]. Therefore, a matrix effort under transverse loading is proposed, relating the dilatational strain energy U_v to the critical value $U_{v,crit}$:

$$e_M = \sqrt{U_v / U_{v,crit}} \tag{6}$$

The dilatational strain energy of the matrix inside a unidirectional layer is given by:

$$U_V = \frac{1-2\nu}{6E}\left(\sigma_I + \sigma_{II} + \sigma_{III}\right)^2 \tag{7}$$

The critical dilatational strain energy $U_{v,crit}$ is derived by inverse calculation from a tensile test of a 90° unidirectional laminate at room temperature. A linear relationship between the dilatational strain energy and the temperature with the same slope as derived for the matrix strength is assumed (see Eq. 14).

4. Results and discussion

4.1. Dilatometry

Fig. 5 shows the experimentally determined data from the dilatometric measurements for the CTEs of the neat resin and the unidirectional reinforced polymer. Each measurement has been repeated four times and a very good coincidence between the measurements has been observed.

In the temperature range of 200 K to 350 K, which is below the glass transition temperature of the resin, a linear dependence of the CTE of the neat resin with respect to the temperature has been observed. The glass transition temperature has been determined to be 356 K by DSC measurements. Hence, the CTE of the matrix $\alpha_{T,M}$ has been determined by linear fitting of the experimental data to:

$$\alpha_{T,M}(T) = 9,29 \cdot 10^{-8} K^{-2} \cdot T + 3,10 \cdot 10^{-5} K^{-1} \tag{8}$$

Since an experimental determination of the CTE of the pure glass fiber is difficult, it is obtained by inverse calculation from the CTE of the longitudinal reinforced composite using the micro-mechanical formulation according to Schürmann [25] by inverting Eq. 9, which leads to Eq.10:

$$\alpha_{T,\parallel} = \frac{\varphi \cdot E_F \cdot \alpha_{T,F} + (1-\varphi) \cdot \alpha_{T,M} \cdot E_M}{\varphi \cdot E_F + (1-\varphi) \cdot E_M} \tag{9}$$

$$\alpha_{T,F} = \frac{\alpha_{T,\parallel} \cdot \left(\varphi \cdot E_F + (1-\varphi) \cdot E_M\right) - (1-\varphi) \cdot \alpha_{T,M} \cdot E_M}{\varphi \cdot E_F} \tag{10}$$

The temperature-dependent formulation for the elastic modulus of the matrix E_M given in Eq. 13 has been used. For the modulus of the fiber E_F, the value of $E_F = 81250\ MPa$ was calculated based on inverse evaluation of tensile tests with 0° reinforced unidirectional specimens. The fiber volume fraction of the dilatometer specimens of $\varphi \approx 0.48$ was lower than the reference volume fraction of 0.55 of the tensile test specimens.

The resulting CTE of the fiber $\alpha_{T,F}$ is also dependent on temperature. This observation matches findings from literature [26,27]. The CTE of the glass fiber $\alpha_{T,F}$ results to:

$$\alpha_{T,F}(T) = 1.41 \cdot 10^{-8} K^{-2} \cdot T + 1.48 \cdot 10^{-6} K^{-1} \tag{11}$$

The CTEs of the composite may now be calculated dependent on the temperature and fiber volume fraction according to Eq. 9 and Eq.12:

$$\alpha_{T,\perp} = \varphi \cdot \alpha_{T,F} + (1-\varphi) \cdot \alpha_{T,M} \tag{12}$$

The calculated CTEs according to Eq. 9 and Eq. 12 are compared with the experimental data in Fig. 6 to validate the inverse determined CTE of the fiber $\alpha_{T,F}$ given in Eq. 11. The results show a good correlation for both the CTE in 0° and in 90° direction of the composite.

4.2. Quasi-static tests

Quasi-static tensile tests have been performed with neat resin specimens, as well as unidirectional and multidirectional reinforced laminates.

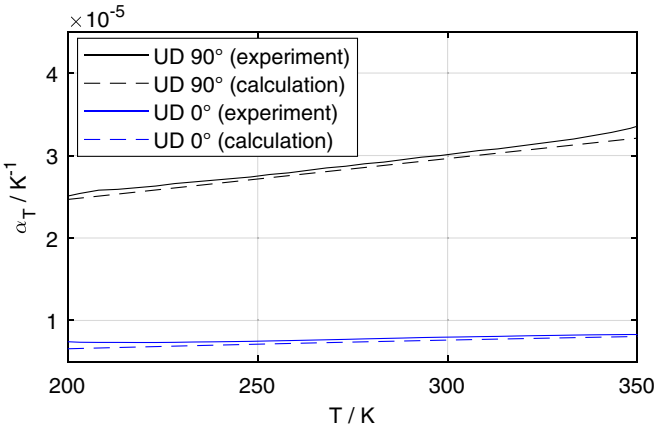

Fig. 6. Comparison of the experimentally determined CTE and the calculations.

4.2.1. Neat resin

The results of the neat resin tests are shown in Fig. 7 for the elastic moduli. The reinforcing effect of the strain gauges leading to a higher measured stiffness is clearly visible.

The strength of the resin has also been evaluated and shown in Fig. 8.

Following the linear regression, the elastic modulus of the resin depending on the temperature results to:

$$E_M(T) = \left(-11,588\ MPa \cdot K^{-1}\right) \cdot T + 6274,7\ MPa \tag{13}$$

Here, only the extensometer measurements have been considered, so the reinforcing effect of the strain gauges has no impact on the obtained modulus.

For the strength of the neat resin, only the specimens without strain gauges have been considered, because the strain gauge leads to a notch-like effect that induces a premature failure of the specimens. From the data without strain gauges follows:

$$R_M(T) = \left(-0,6504\ MPa \cdot K^{-1}\right) \cdot T + 258,8\ MPa \tag{14}$$

4.2.2. 90°-unidirectional reinforced specimens

The evaluated transverse elastic moduli of the unidirectional reinforced specimens $E_\perp(T)$ are shown in Fig. 9. The calculated values with

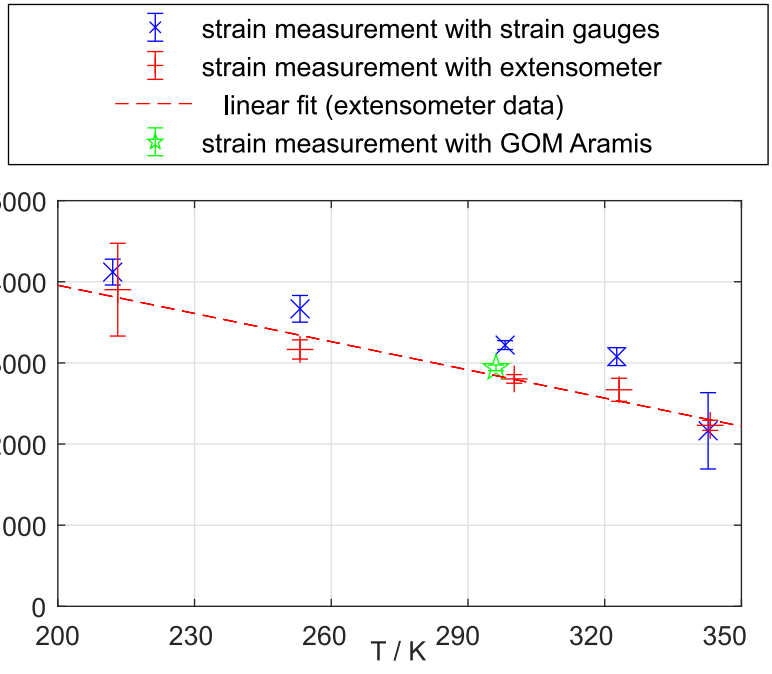

Fig. 7. Elastic modulus of the neat resin.

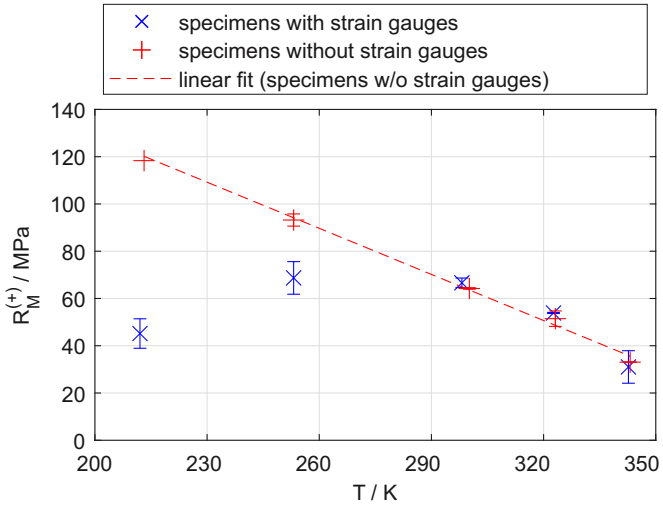

Fig. 8. Strength of the neat resin.

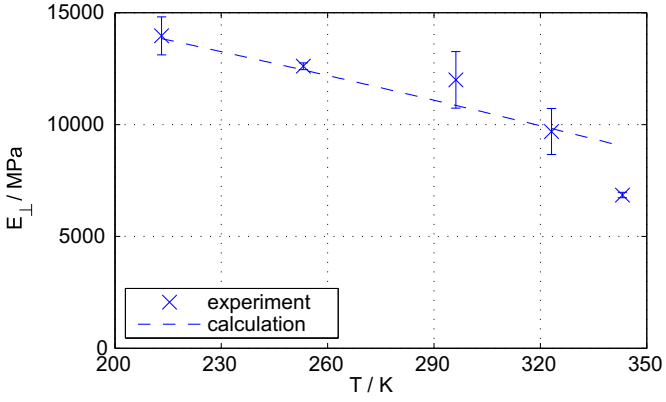

Fig. 9. Transverse modulus of the unidirectional layer.

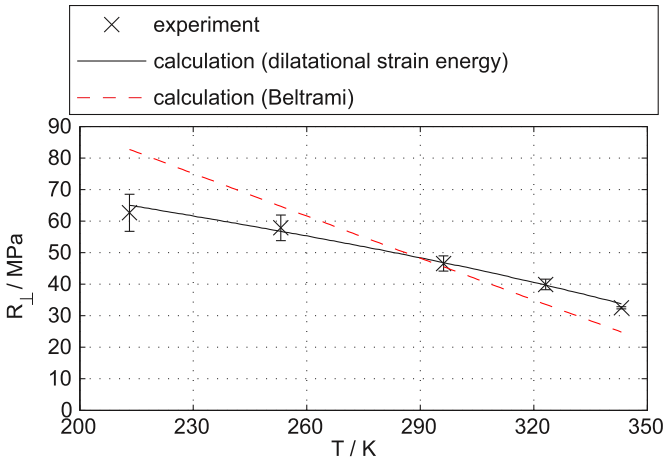

Fig. 10. Transverse strength of the unidirectional layer.

the formulae according to Krimmer based on the properties of the neat resin and the fiber as described above, are shown by the dashed line. The experimental values show an overall good correlation to the calculated ones. The experimental values at room temperature are higher than expected and the scatter of the values is relatively high. However, the calculated values are still inside the variance of the experimental data. The higher experimentally measured modulus may be caused by the strain measurement which was performed using strain gauges. Thus, the obtained data is highly sensitive to possible local inhomogeneities of the specimen at the position of the strain gauge. Furthermore, the reinforcing effect of the strain gauges, that has been discussed in Section 4.2.2 may have also influenced the measurement of the transverse modulus. The values at 343 K are lower, most likely due to the beginning of the glass transition influence.

The experimentally determined transverse strength values $R_\perp(T)$ for the unidirectional layer are shown in Fig. 10. The strength was calculated by computing the matrix effort according to Eq. 4 and Eq. 6. It was assumed that the static strength of the unidirectional specimen is reached at a matrix effort of $e_M = 1$. For comparison, the calculated strength using the Beltrami criterion according to Krimmer as well as the dilatational strain energy criterion is shown. The latter shows an excellent correlation with the experimental data.

4.2.3. 0°/90°-Specimens

Fig. 11 shows the damage evaluation and the strain for an exemplary test of an 0°/90° reinforced specimen at room temperature with respect to the axial laminate stress σ_x. The undamaged specimen (a) gets loaded with a linear increase in strain. A progressive increase of the damage parameter is detected due to micro-cavitation inside the matrix, but no macroscopic damage is visible.

At point (b), first macroscopic transverse cracks become visible. At point (c), several cracks are forming and a decrease in stiffness caused by the degradation of the transverse layers is detected. At point (d), a saturation of the transverse cracks is reached. The spike in the strain curve between (c) and (d) may be related to first fiber damage, which is not detected in terms of the optical damage parameter. The specimen fails in point (e) due to a sudden death caused by multiple fiber fractures in the longitudinal layers.

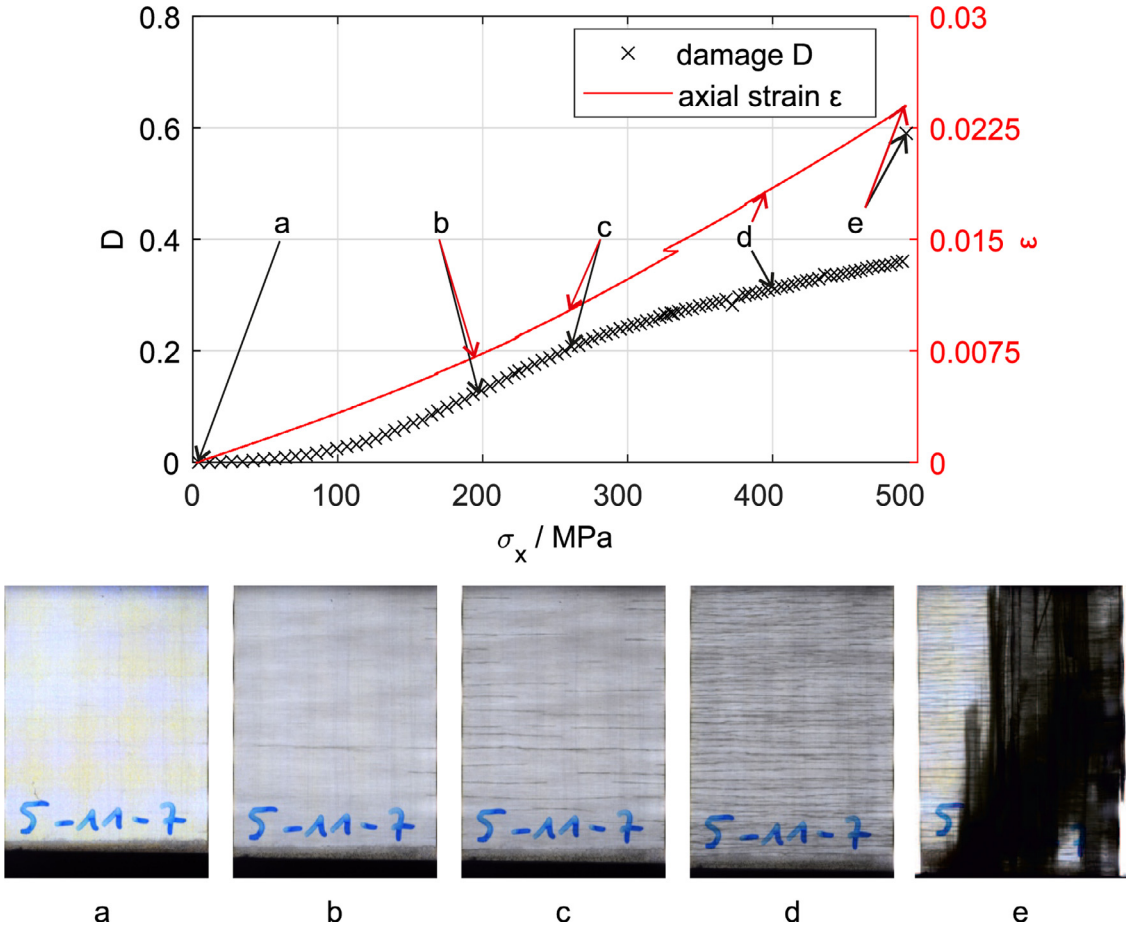

Fig. 11. Damage evolution at 0°/90° reinforced specimen at room temperature.

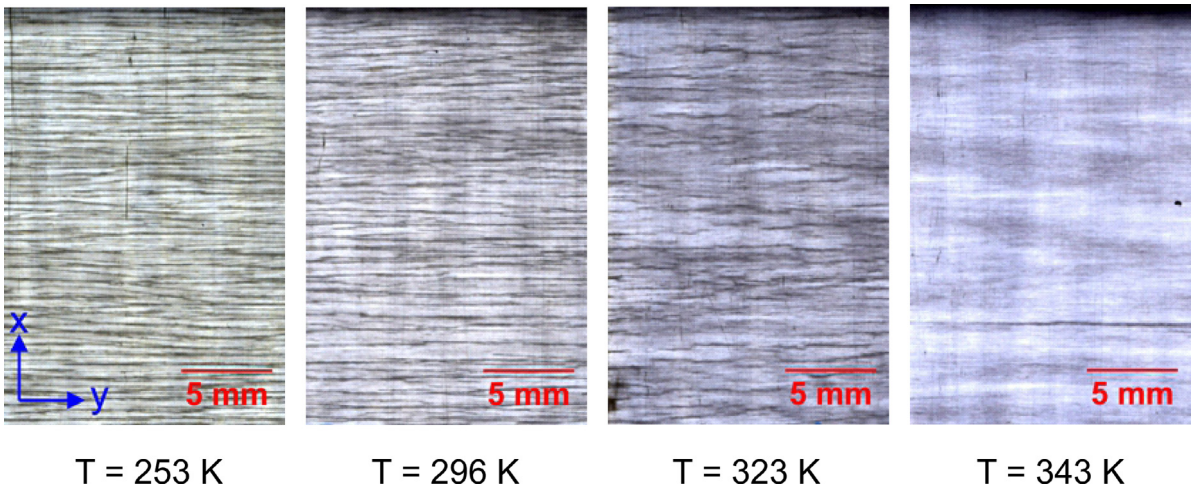

Fig. 12. Damage state before fiber fracture at different temperatures.

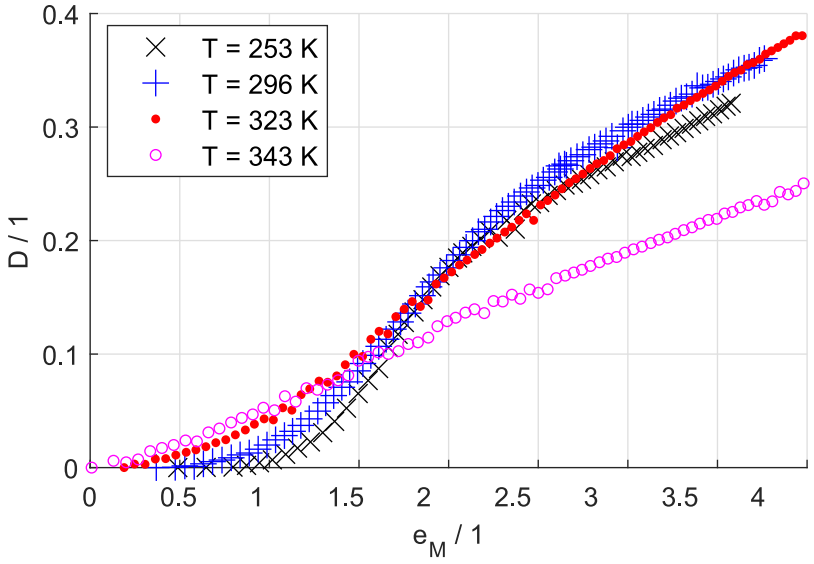

Fig. 13. Damage evolution dependent on the temperature.

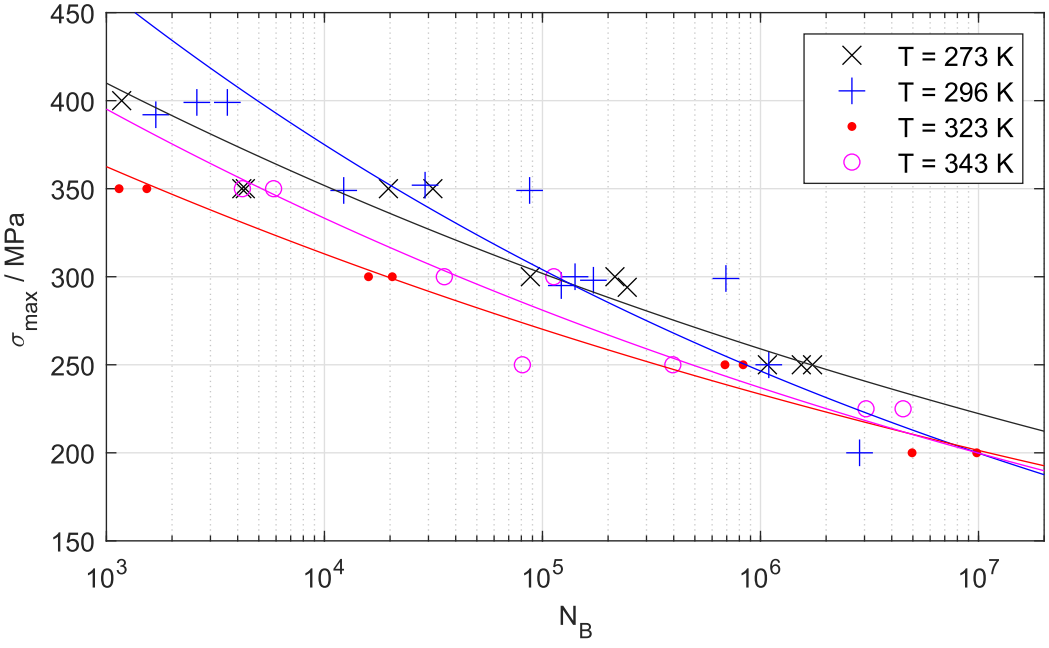

Fig. 14. S-N-curves for 0°/90° specimens under fatigue loading; $R = 0.1$.

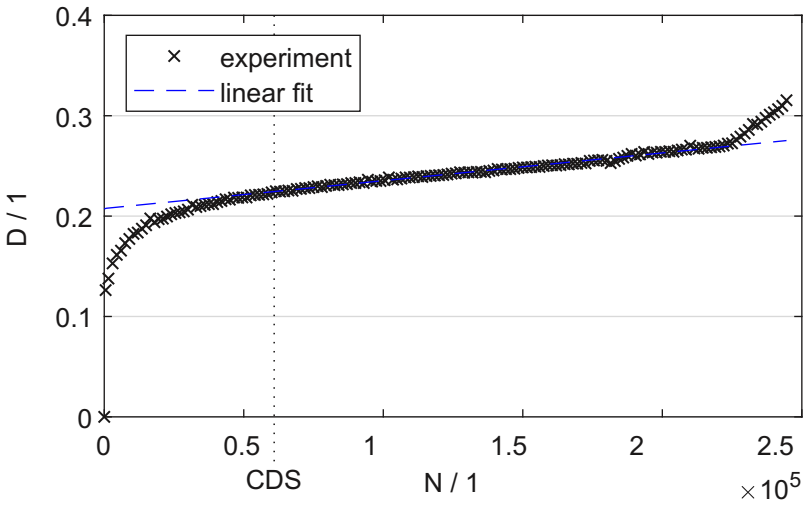

Fig. 15. Determination of the CDS based on the optical damage measurement.

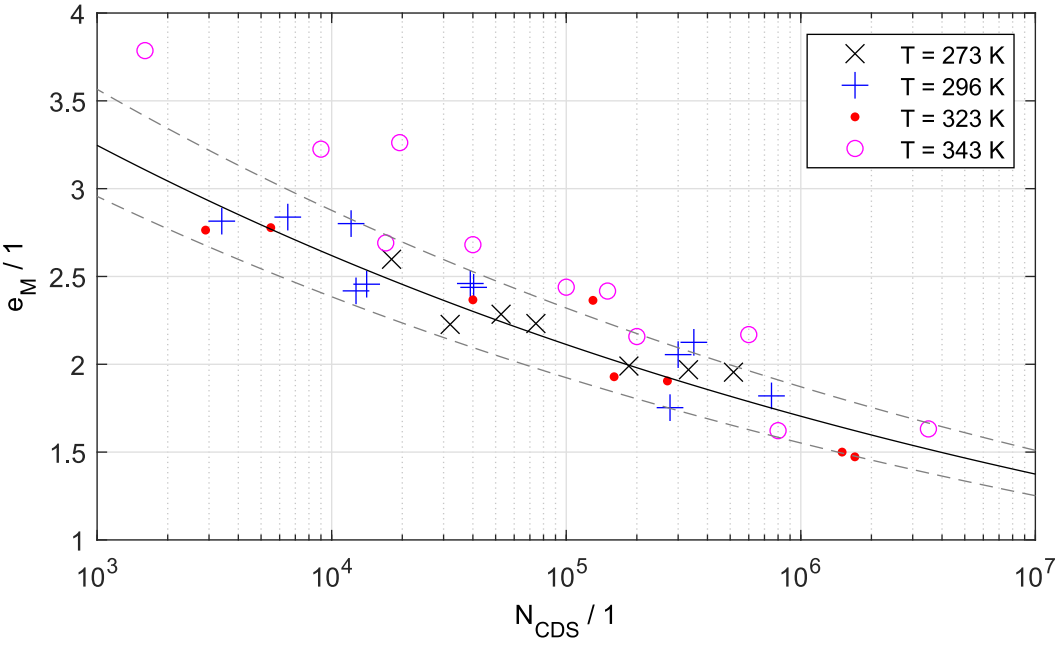

Fig. 16. Master-fatigue-curve for 0°/90° specimens under fatigue loading; $R = 0.1$.

The damage progression is similar at lower and higher temperatures, but the phenomenology of the transverse cracks varies. Fig. 12 shows pictures of samples at different temperatures just before global fiber failure is detected. At colder temperatures, transverse cracks are going straight through the specimens, while at higher temperatures more shorter cracks are detected. Therefore, it is suspected, that the matrix can stop the cracks at higher temperatures. At low temperatures, the brittle matrix leads to a very unstable crack propagation. At 343 K, no macroscopic cracks have been detected. Rather, smaller cracks, which are widely spread all over the specimen, could be seen.

Fig. 13 shows the damage parameter D related to the matrix effort e_M, calculated by means of the critical dilatational strain energy. A nearly temperature-independent correlation could be observed for values of $e_M > 1.5$, except for the specimens tested at 343 K. In theory, the first damage would be expected at a value of $e_M = 1$. The experimental data at $e_M = 1$ shows a variance in the optical parameter and a temperature-dependency in the obtained damage values. At $T = 253\ K$, the growth of the damage parameter D starts around $e_M = 1$, which is in line with the theoretical expectations. At higher temperatures, a premature increase of the damage parameter is observed. This is connected to the temperature-dependent damage modes shown in Fig. 12. While no macroscopic cracks with widths of 15 µm to 100 µm are observed at values of $e_M < 1$ at any temperature level, the damage parameter of the specimens tested at higher temperatures starts increasing because of microscopic cracks with widths smaller than 10 µm leading to a higher grey scale value of the specimens.

4.2.4. Fatigue tests

The damage parameter D has been measured during the fatigue tests by means of optical transmission analysis, as shown in Fig. 4. The numbers of cycles until complete failure of the specimen N_B dependent on the temperature and the maximum laminate stress σ_{max} are shown in the S-N plot in Fig. 14. A tendency to longer fatigue life with lower temperatures is visible, but no distinct correlation can be seen.

The CDS has been described by Reifsnider et al. as the damage state where the specimen is saturated with transverse cracks [28]. The CDS

has been evaluated based on the optical transmission measurements. This is shown exemplarily for a measurement at room temperature in Fig. 15. A linear fit for the damage parameter in the range of $0.2 \leq N/N_B \leq 0.8$ is performed, which is represented by the dashed line. The CDS is identified at the intersection between this linear fit and the experimentally determined damage curve.

To evaluate the correlation between damage, temperature and fatigue life, the number of cycles until the characteristic damage state (CDS) n_{CDS} is reached has been plotted versus the maximum matrix effort e_M calculated according to Eq. 6 with the dilatational strain energy criterion in Fig. 16. Taking the CDS into account instead of fiber fracture considers the matrix damage more and reduces the scatter in the evaluated fatigue life values. Fig. 16 shows the obtained $e_M - N_{CDS}$ curves. It can be seen that the specimen data obtained at all temperatures except for the highest temperature at 343 K forms one temperature-independent master S-N curve, which is shown by the continuous line. The dashed lines show the probabilities of failure of 90% and 10% for the temperature range from 273 K to 323 K.

5. Conclusion

It was demonstrated that the thermo-mechanical properties of the transverse unidirectional layers of the glass fiber reinforced polymer can be calculated based on the properties of its constituents with the micromechanical formulations. The temperature dependence of the matrix properties leads to a temperature dependence of the overall composite properties. In particular, the temperature-dependent transverse strength can be determined by means of the critical dilatational strain energy criterion.

The damage progression under quasi-static loading can be related to the nominal matrix effort based on the linear elastic model. This is not valid at high temperatures in the vicinity of the glass transition temperature. The validity of these observations needs to be checked for other materials. While the formulae may be taken for any isotropic fiber materials, an adoption for anisotropic fibers like carbon fibers has been performed by Müller [29]. The correlation between matrix effort and damage has been evaluated under tensile loading. Other damage mechanisms are expected under compressive loading. Compressive failure of GFRP bars is investigated by Abed et al. [30]. On a smaller specimen scale, the compressive damage behavior has been investigated by Berbinau et al. for carbon fiber reinforced specimens [31].

The matrix effort is also a crucial factor for the fatigue strength of the laminate. The fatigue properties of the 0°/90° laminate can be estimated by means of a master fatigue curve, taking the characteristic damage state and the matrix effort into account. Even though the linear elastic model describes only the undamaged continuum, an estimation of the fatigue life under transverse loading is possible based on the nominal stress state of the matrix. The demonstrated correlations are only valid for temperatures sufficiently below the glass transition. Since fatigue experiments at low temperature conditions are not trivial, the obtained master fatigue curves allow an estimation of the fatigue life in a preliminary design phase with a very low experimental effort for a wide temperature range for transverse loaded specimens.

Declaration of Competing Interest

The authors declare that they have no known competing financial interests or personal relationships that could have appeared to influence the work reported in this paper.

Acknowledgements

The work was funded by the Deutsche Forschungsgemeinschaft [grant no. TR 499/5-1, title „Schädigung von Faser-Kunststoff-Verbunden infolge des inneren multiaxialen Spannungszustandes, hervorgerufen durch äußere thermische, (multiaxiale) mechanische und feuchte Ermüdungsbeanspruchung“]

The authors would like to thank Stefan Hickmann, Lothar Buchta and Matthias Ell for their help with the performance of the experiments, and Adrian Fried, Frederick Fuchs, Julian Marzik and Julia Ziegler for their assistance with the preparation of the specimens. The authors gratefully acknowledge the proofreading of the manuscript by Carineh Ghafafian.

References

[1] HT. Hahn, Residual stresses in polymer matrix composite laminates, J. Compos. Mater. 10 (1976) 266–278, doi:10.1177/002199837601000401.
[2] B Fiedler, T Hobbiebrunken, M Hojo, K. Schulte, Influence of stress state and temperature on the strength of epoxy resins, in: Proc. 11th Int. Conf. Fract. ICF 11, Torino, Italy, 2005, pp. 2271–2275.
[3] P Jenkins, S Riopedre Mendez, E Saez Rodriguez, L Yang, J Thomason, Investigation of the strength of thermally conditioned basalt and e-glass fibres, 20th Int. Conf. Compos. Mater, 2015.
[4] C Sauder, J Lamon, R. Pailler, The tensile behavior of carbon fibers at high temperatures up to 2400°C, Carbon 42 (2004) 715–725, doi:10.1016/j.carbon.2003.11.020.
[5] MM Shokrieh, SM Kamali Shahri, Modeling residual stresses in composite materials, in: MM Shokrieh (Ed.), Residual Stress. Compos. Mater., Woodhead Publishing, 2014, pp. 173–193, doi:10.1533/9780857098597.1.173.
[6] A. Puck, Festigkeitsanalyse von Faser-Matrix-Laminaten: Modelle für die Praxis, Hanser, 1996.
[7] Alexander Krimmer, Rico Leifheit, Andreas Bardenhagen, Assessment of quasi-static and fatigue performance of uni-directionally fibre reinforced polymers on the basis of matrix effort, 6th EASN Int. Conf. Innov. Eur. Aeronaut. Res., Porto, 2016.
[8] A. Krimmer, Mikromechanische Modellierung von Fasergelege-Kunststoff-Verbunden auf Basis von Normprüfungen unter Berücksichtigung der in-situ-Eigenschaften der Matrix, Universitätsverlag der TU Berlin, Berlin, 2014.
[9] Kraus D. Ermüdungsverhalten von Glasfaser-Kunststoff-Verbunden unter thermomechanischer Beanspruchung. Berlin: 2021.
[10] S Adden, P. Horst, Damage propagation in non-crimp fabrics under biaxial static and fatigue loading, Compos. Sci. Technol. 66 (2006) 626–633, doi:10.1016/j.compscitech.2005.07.034.
[11] D Munzke, D Kraus, R Eisermann, S Kübler, M Schukar, L Nagel, S Hickmann, V Trappe, Distributed fiber-optic strain sensing with millimeter spatial resolution for the structural health monitoring of multiaxial loaded GFRP tube specimens, Polym. Test (2019) 106085, doi:10.1016/j.polymertesting.2019.106085.
[12] ISO 527-2:2012-02 Plastics - Determination of tensile properties - Part 2: Test conditions for moulding and extrusion plastics. 2012.
[13] A Ajovalasit, B. Zuccarello, Local reinforcement effect of a strain gauge installation on low modulus materials, J. Strain Anal. Eng. Des. 40 (2005) 643–653, doi:10.1243/030932405X30894.
[14] EG Little, D Tocher, P O'Donnell, Strain gauge reinforcement of plastics, Strain 26 (1990) 91–98.
[15] ISO 527-5:2009-07 Plastics - Determination of tensile properties - Part 5: Test conditions for unidirectional fibre-reinforced plastic composites. 2009.
[16] A Müller, V Trappe, S Hickmann, H-P. Ortwein, Investigation of the infinite life of fibre-reinforced plastics using X-ray refraction topography for the in-situ, non-destructive evaluation of micro-structural degradation processes during cyclic fatigue loading, in: H-J Christ (Ed.), Fatigue Mater. Very High Numbers Load. Cycles Exp. Tech. Mech. Model. Fatigue Life Assess., Springer, Wiesbaden, 2018, pp. 417–439, doi:10.1007/978-3-658-24531-3_19.
[17] GA Abu-Farsakh, SA Barakat, FH. Abed, A Macromechanical Damage Model of Fibrous Laminated Composites, Appl. Compos. Mater. 6 (1999) 99–119, doi:10.1023/A:1008882909136.
[18] V Trappe, S Hickmann, H. Sturm, Evaluation of inter fibre fracture in textile glass fibre composites by X-ray refraction topography, Mater. Test. 50 (2008) 615–622, doi:10.3139/120.100923.
[19] B Fiedler, M Hojo, S Ochiai, K Schulte, M. Ochi, Finite-element modeling of initial matrix failure in CFRP under static transverse tensile load, Compos. Sci. Technol. 61 (2001) 95–105, doi:10.1016/S0266-3538(00)00198-6.
[20] R Talreja, CV. Singh, Damage and Failure of Composite Materials, Cambridge University Press, 2012.
[21] Beltrami E. Sulle condizioni di resistenza dei corpi elastici. Il Nuovo Cimento 1877-1894 1885;18:145–155. https://doi.org/10.1007/BF02824697.
[22] LE Asp, LA Berglund, R. Talreja, A criterion for crack initiation in glassy polymers subjected to a composite-like stress state, Compos. Sci. Technol. 56 (1996) 1291–1301, doi:10.1016/S0266-3538(96)00090-5.
[23] LE Asp, LA Berglund, R. Talreja, Prediction of matrix-initiated transverse failure in polymer composites, Compos. Sci. Technol. 56 (1996) 1089–1097, doi:10.1016/0266-3538(96)00074-7.
[24] LE Asp, LA Berglund, P. Gudmundson, Effects of a composite-like stress state on the fracture of epoxies, Compos. Sci. Technol. 53 (1995) 27–37, doi:10.1016/0266-3538(94)00075-1.
[25] H. Schürmann, Konstruieren mit Faser-Kunststoff-Verbunden, Springer-Verlag, 2007.
[26] NP Bansal, RH. Doremus, Handbook of Glass Properties, Elsevier, 2013.
[27] A. Fluegel, Thermal expansion calculation for silicate glasses at 210°C based on a systematic analysis of global databases, Glass Technol. Eur. J. Glass Sci. Technol. Part A 51 (2010) 191–201.

[28] Reifsnider KL, Henneke EG, Stinchcomb WW. Defect-Property Relationships in Composite Materials. Part III. VIRGINIA POLYTECHNIC INST AND STATE UNIV BLACKSBURG; 1978.
[29] Müller A. Schädigungscharakterisierung an Faser-Kunststoff-Verbunden im Schwingversuch mittels Röntgenrefraktionstopographie unter Berücksichtigung der Matrixeigenschaften. Berlin: 2018.
[30] F Abed, Z Mehaini, C Oucif, A Abdul–Latif, R Baleh, Quasi-static and dynamic response of GFRP and BFRP bars under compression, Compos. Part C Open Access 2 (2020) 100034, doi:10.1016/j.jcomc.2020.100034.
[31] P Berbinau, C Soutis, IA. Guz, Compressive failure of 0° unidirectional carbon-fibre-reinforced plastic (CFRP) laminates by fibre microbuckling, Compos. Sci. Technol. 59 (1999) 1451–1455, doi:10.1016/S0266-3538(98)00181-X.